

Detection of arcs in Saturn's F ring during the 1995 Sun ring-plane crossing

S. Charnoz¹, A. Brahic¹, C. Ferrari¹, I. Grenier¹, F. Roddier², P. Thébault³

¹ Equipe Gamma-Gravitation, Service d'Astrophysique, CEA/Saclay, Orme des Merisiers, 91191 Gif sur Yvette cedex, France

² Institute for Astronomy, University of Hawai, 2680 Woodlawn Drive, Honolulu, Hawaii 96822

³ DESPA, Observatoire de Paris, 92195 Meudon Cedex Principal, France

Received date / Accepted date

Abstract. Observations of the November 1995 Sun crossing of the Saturn's ring-plane made with the 3.6m CFH telescope, using the UHAO adaptive optics system, are presented here. We report the detection of four arcs located in the vicinity of the F ring. They can be seen one day later in HST images. The combination of both data sets gives accurate determinations of their orbits. Semi-major axes range from 140 020 km to 140 080 km, with a mean of $140\,060 \pm 60$ km. This is about 150 km smaller than previous estimates of the F ring radius from Voyager 1 and 2 data, but close to the orbit of another arc observed at the same epoch in HST images.

Key words: Planets: individual : Saturn's rings

1. Introduction

The Sun's crossing of Saturn's ring-plane is a rare opportunity to observe the unlit face of the rings. Results of observations made at the 3.6m CFH Telescope are reported here. Thanks to the use of the UHAO adaptive optics system (Roddier et al. 2000), high resolution ground-based images were obtained ($\sim 0.15''$ in August 1995 and $\sim 0.25''$ in November 1995). The Sun's crossing lasted from November 17th to 21st 1995. It was accompanied by three Earth ring plane crossings (1995 May 22nd, August 10th, and 1996 February 11th). Several teams observed these events (Nicholson et al. 1996, hereafter N96; Bosh & Rivkin 1996; Sicardy et al. 1996; Roddier et al. 1996a; Ferrari et al. 1997).

The unusual viewing of the rings during these events provides a rare opportunity to detect faint structures such as small satellites, clumps, or arcs, that are usually lost in the glare of the bright main rings. In this paper, we focus our attention on the azimuthal structure of the F ring. Located at the Roche limit of Saturn and bounded by two shepherding satellites Pandora and Prometheus,

the F ring is very intriguing. The Voyager images revealed its complex radial and azimuthal structure including multiple strands, clumps and braids. Interactions with Saturn's satellites might explain some features, but they are not completely understood.

During the 1995 ring crossing observing campaign, the F ring appeared populated with numerous features, either point-like or longitudinally extended. The observation of two point-like objects (S/1995 S1 and S/1995 S3) was reported by Bosh & Rivkin (1996) during the May crossing. During the August crossing, our team discovered at least 6 new features with semi-major axes compatible with the F ring (Roddier et al. 1996a; Ferrari et al. 1997). At least one of them was identified as an arc-like object. During the same period three objects (S/1995 S5, S/1995 S6 and S/1995 S7) were detected by N96. Finally, during the November crossing, two wide arcs (7° and 10° -long) were observed by N96. The brightest was also seen by Poulet et al. (2000, hereafter P2000). The most striking aspect of those discoveries is that no evident correlation can be found between features observed in May, August and November (N96, Bosh & Rivkin 1996, P2000).

In the present paper, we report the detection of 4 arcs in the region of the F ring on November 20th. The same features can be seen in some HST images taken 24 to 36 hours later. These images have been already presented in N96. By combining both sets of data, accurate orbital solutions are derived. The data processing of CFHT and HST images is presented in the first section. Results are presented in the second section and discussed in the final section.

2. Description of data set and processing

2.1. Description of data

Images were taken at the 3.6m CFH Telescope during four nights from 1995 November 17th to 20th. Three near-infrared filters (J,H and K), which correspond to the absorption bands of methane were used to significantly reduce the strong scattered light of Saturn. A K band image is presented in Fig 1. The best observing conditions

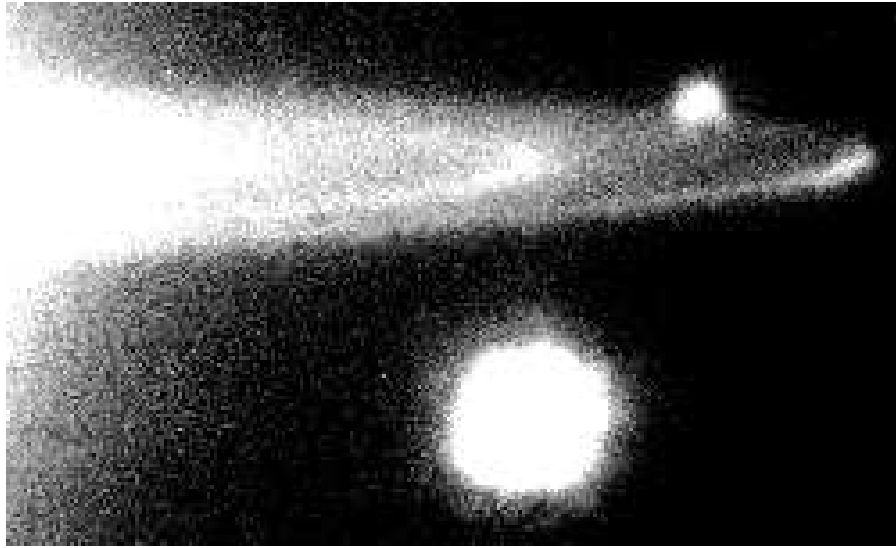


Fig. 1. Image of the West ansa in the K band on 1995 November 21 at 5h11 UTC, obtained at CFHT with the UHAO system. The F ring and the Cassini division appear brightly. Janus (upper right) and Tethys (bottom center) are visible in this image. The north pole of Saturn is oriented toward the top of the image. This image is slightly saturated as can be seen from the Cassini division and the F ring.

were obtained during the last night, the main rings being darkest. During the nights of November 17th, 18th, 19th the stronger brightness of the main rings was not favorable for the detection of dim objects. Consequently only images of November 20th were considered.

At this time the Sun was about 0.01° below the rings, and the Earth was at 2.67° above the ring plane, looking at the unlit face. 160 images of the west ansa were obtained from 5h to 8h45 UT. At this time, there was no satellite on the east ansa bright enough for the adaptive optics tracking system to work properly. In consequence, the CFHT data set contains only images of the west ansa. The resolution has been checked on every image by extracting the point spread function (PSF) of satellites Tethys, Enceladus, Dione and Mimas. The full width at half maximum of the PSF is on average $0.25''$ (1670 km at Saturn) on the whole data set, ranging from $0.19''$ to $0.33''$. The size of one pixel in arcsecond is determined by comparing the angular separation of all pair of major satellites (given by the ephemeris) with their separation in pixels as measured on the plates. The result is robust : one pixel subtends $0.035''$ (~ 233 km at Saturn). The exposure times ranged from 15 s to 30 s.

In order to make a comparative study of two complementary data sets, we have also used the HST images presented in N96, retrieved from the FTP site of the Space Telescope Science Institute. They consist of twenty Planetary Camera images of both ansae (10 images for each ansa), taken with filters centered at 890 nm, between 10h UT and 18h UT on November 21st, at the end of the Sun's crossing. The resolution is $0.1''$ (668 km at Saturn). The scale of the plates is taken from Holtzman et al. (1995):

one pixel subtends $0.045''$ (~ 304 km at Saturn). Exposure times range from 300s to 500s. As a consequence, satellites appear smeared due to their keplerian motion.

2.2. Data processing

Our data processing has been designed for the detection of faint objects in the F ring. As a consequence we have not made a photometric study; indeed many images with different exposure times and different filters are combined indiscriminately. A longitudinal profile of the F ring was built to reveal new objects. To this purpose the following data processing steps were applied to both CFHT and HST images : (i) astrometry, (ii) extraction of the F ring profiles, (iii) subtraction of the F ring background and the correction of geometry and illumination effects.

2.2.1. Astrometry

In CFHT images, the center of Saturn and orientation of the planet's North pole axis is determined by a least square fit to the positions of satellites Tethys, Enceladus, Mimas and Dione (using the ephemeris of the Bureau Des Longitudes in Paris). However Mimas and Tethys could not be used in one third of images in which they are observed too close to each other, not suitable for an accurate determination of their center. In these images the point of maximum elongation of the Cassini division and of the F ring were used to better constrain the orientation of Saturn's equatorial axis. The residual on satellites position measurements is $0.09''$ (~ 2.6 pixels or 600 km), and reflects a combination of pointing and

ephemeris errors.

In HST images, the astrometry has not been done using satellites because of their elongated appearance. The sharp inner edge of the Cassini Division was used instead as a reference. Located at 117 577 km from the center of Saturn, it is known to be slightly eccentric due to the close 2:1 resonance with Mimas. The resulting radial excursion ($2ae$) is only 150 km, representing 0.5 pixel, or $0.02''$ (Porco et al. 1984). The center of Saturn as well as the orientation of the axes are determined by fitting an ellipse with twenty points picked by eye on the reference edge. Corrections of the geometrical distortion for WF/PC2 camera (WF/PC2 instrument handbook version 5.0, provided by the STSCI) is included only when new objects are measured, for the need of their orbit determination. The astrometric error is determined from the residuals of the Cassini division fit. It is $0.035''$ (~ 0.8 pixel or 240 km at Saturn). The correction for geometrical distortion is about 1 pixel, representing less than 0.6° on the F ring longitudinal profile, not detectable in Fig 2 and Fig 3.

2.2.2. Extraction of the F ring profile

From -55° to $+55^\circ$ around maximum elongation, pixel counts are summed perpendicularly to the equator axis, in a box centered on the F ring (defined as a circle of radius 140 200 km and projected onto the ring plane) with the same width as the PSF. For each image, an intensity profile of the F ring is obtained as a function of longitude, measured from the point of maximum elongation. The extremity of the ansa (within 5 pixels around maximum elongation) is not considered because the scans become parallel to the ring in this region. The scattered light of Saturn is estimated in the neighborhood of the integration box, outside the F ring, and systematically subtracted. Profiles are then corrected for effects of the different filters and for different exposure times: each profile is multiplied by a normalization factor in order to keep at the same median level of brightness a reference zone of the F ring, chosen to be between 0° and 45° before maximum elongation. Because of the low opening angle of the rings system, the reference zone is slightly contaminated by the A ring beyond 25° from maximum elongation. However we have checked that all profiles do not present systematic deviations in the reference zone after this operation.

2.2.3. Subtraction of the F ring background and correction of illumination effects

A synthetic median profile (SMP) of the F ring is built by taking the median value of all profiles at each longitude relative to elongation. The SMP is a template of the F ring. It is subtracted from all profiles in order to reveal local brightness variations.

The apparent brightness of the F ring changes along its path around the ansa due to geometrical effects (the length of a ring segment included in one pixel depends on longitude) and probably to shadowing by the A ring (N96). Indeed the F ring brightness decreases abruptly after maximum elongation on the west ansa, as noticed in N96. To correct for these effects and maintain embedded features at a constant level of brightness, all profiles are divided by the SMP. Taking into account the subtraction of the F ring background, all profiles are processed according to the formula: Final Profile = $(profile - SMP)/SMP$. Dividing by the SMP increases noise in dim regions. This method preserves the brightness of objects within 20% before and after their passage through the maximum elongation (as observed on arcs B,C and on the 10° arc of N96, see below) and allows tracking of objects.

2.2.4. Construction of the longitudinal F ring profile

Each (final) profile is precessed to the standard epoch of November 21.5 TDT (terrestrial dynamic time) at Saturn, with a mean orbital motion of $582.05^\circ/\text{day}$ (N96). This allows direct comparison with N96 results. Finally a mean longitudinal profile is computed by averaging all precessed profiles.

The resulting CFHT and HST profiles are presented in Fig. 2. The derived HST full azimuthal profile (see Fig. 2.c) is in close agreement with the one published in N96, in terms of the positions of objects and relative brightnesses, although our profile may appear somewhat noisier than the one published in N96. In this profile, the correction for the distortion of the WF/PC2 camera has not been considered, resulting in an azimuthal error less than $\sim 0.6^\circ$. The vertical axis is scaled such that the maximum intensity of Pandora, as observed in the processed profiles, equals 1.

3. Results

In this section the F ring azimuthal profile obtained from CFHT observations is described and compared with the HST profile. Orbital solutions for four detected structures are then calculated.

3.1. F ring longitudinal profile and new objects

3.1.1. CFHT images

The complete azimuthal coverage of the data set ranges between 50° to 230° . But the region extending from 50° to 80° has been covered by only a few suitable images (~ 10) and is deeply embedded in the very strong scattered light of Saturn's globe. Apart from Pandora appearing at 62° , nothing is detected below 80° . Janus contaminates CFHT profiles around 210° longitude. The region of interest then extends between 80° and 200° (Fig 2.a). In this range, the

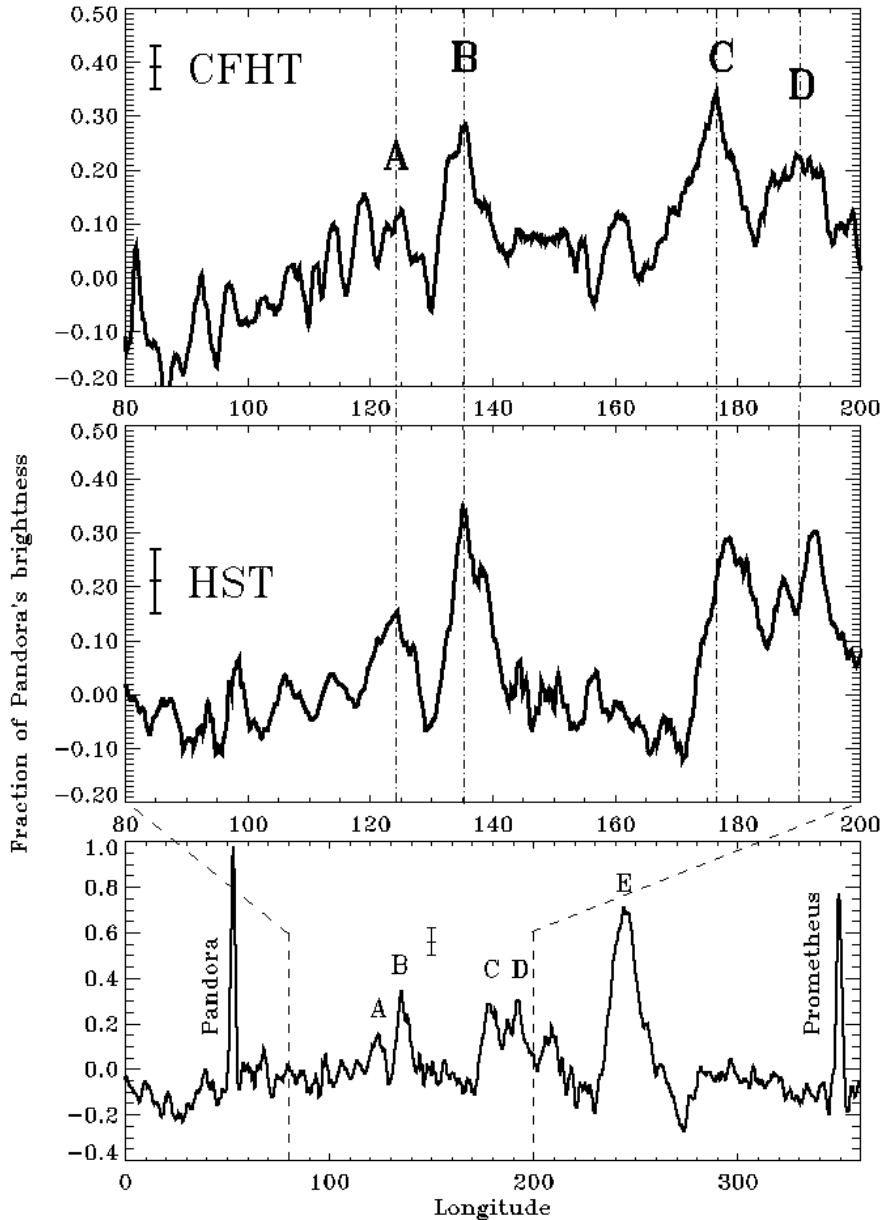


Fig. 2. Longitudinal brightness profiles extracted from 160 CFHT images of the west ansa and 20 HST images of both ansae (2.a and 2.b respectively) in the common longitudinal range. Fig 1.c is the full HST profile with complete azimuthal coverage, obtained with our data processing. Error bars are $\pm 1\sigma$. Negative values mean that brightness is locally lower than the background of the ring. All profiles are precessed to the standard epoch 1995 November 21.5 TDT at Saturn. The B and E arc are referred by N96 as the “7° arc” and the “10° arc” respectively. The orbit of the E arc has been determined by P2000.

average error bar (1σ) is about 4% of Pandora’s brightness.

Two structures (B and C) are detected with more than 5σ confidence level, with mean central longitudes of 135° and 177° respectively. The B object is the “7° arc” in N96. Their maximum brightness is 30% to 40% of Pandora’s. Compared to the 3° -azimuthal extension of a point-like source due to the PSF (as observed for Pandora), it is

clear that B and C are azimuthally extended objects. The B object has a FWHM of $\sim 7^\circ$. It is observed before (from 5h10 to 6h30 UT) and after its passage through maximum elongation (from 7h40 to 8h45 UT). Feature C has a FWHM of 10° . It is detected during 20 minutes before maximum elongation (from 5h10 to 5h30) and during 80 mn after maximum elongation (from 5h50 to 7h10 UT). A few other bumps also seem to appear with lower con-

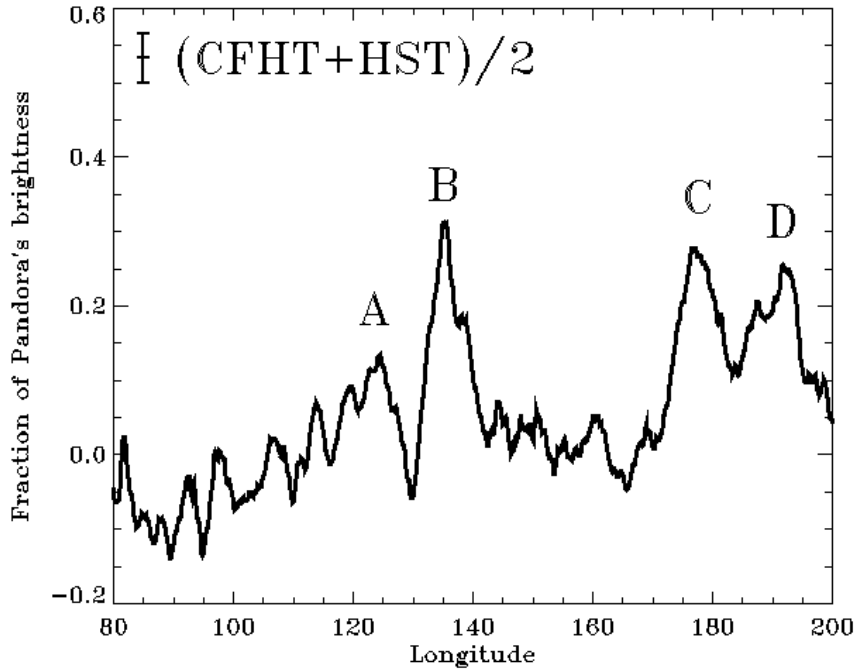


Fig. 3. Mean of CFHT and HST profiles presented in Fig. 2.a. and Fig. 2.b. in the common azimuthal region at the standard epoch. Error bar is $\pm 1\sigma$.

confidence level ($\sim 2-3\sigma$) below 120° and at 124° , 163° and 190° . Only two of them may be tracked on many images with a keplerian motion. The A object, located at 124° , is nearly marginal here and seems to extend from 117° to 129° and has an intensity about 15% of Pandora’s. It is detected from 5h50 to 6h40 UT (~ 30 images). The D object (located at 190°) may be followed from 5h40 to 6h20 UT. Its azimuthal shape is uncertain because of numerous nearby artifacts on the images where it is detected.

3.1.2. Comparison with HST data

Comparison of CFHT and HST profiles indicates that at least structures B and C lasted over a 24 to 36 hours time interval. Indeed both profiles are in good agreement within 1σ (see Fig. 2.a and Fig. 2.b). Because of the small number of images, the noise varies significantly with longitude in the HST profile, depending on the number of images covering each region. It is on average $\sim 6\%$ of Pandora’s brightness. The azimuthal extension of a point-like object is also 3° (measured on Pandora and Prometheus), but here it is mainly due to smearing. Objects B and C are present in both profiles. The shape and position of object B fits particularly well. C appears slightly narrower in the HST profile, but both are compatible within 1σ in intensity. Its FWHM is about 9° in the HST profile.

A better signal to noise ratio is simply obtained by averaging CFHT and HST profiles (see Fig. 3). The new error bar at 1σ is 3.3% of Pandora’s brightness, which im-

proves by factors 1.2 and 1.8 upon the signal to noise ratio of CFHT and HST profiles respectively. In the averaged profile the confidence level of objects B and C increases to 9σ and 8σ respectively. Objects A and D, that were marginal in the CFHT profile, appear now at 5.5σ and 5σ respectively, showing these are real structures. Whereas the shape of A is in good agreement between CFHT and HST profiles, the shape of D is more peaked in the HST profile, and is centered at 192° . Features below 120° and at 164° are comparable to the error bar in the averaged profile. The simultaneous presence of structures A,B,C,D with same positions and similar shapes in both CFHT and HST data confirms that these are real and extended objects. They are designated as “arcs” hereafter.

3.2. Orbital fit

The computation of orbital solutions has been performed using moments J2 to J4 of Saturn’s potential (Campbell & Anderson 1989). The location of objects A,B,C and D are measured on the profiles where the Saturn’s scattered light and the template of the F ring (the SMP) has been subtracted. The center is determined “by eye” by comparing at least three successive profiles where a given object appears clearly. Positions are then converted into distance from the center of Saturn projected onto the planet’s equatorial axis. For HST data, profiles in which objects are measured are corrected for the distortion of the PC camera. Only the best points were considered with the longest

Table 1. CFHT data points of arcs A,B,C,D upon which orbital solutions were determined. The distance (in km) is measured from Saturn’s center, projected perpendiculary on the equatorial axis of the west ansa. The longitude is calculated on the basis of orbital solutions given in Table 2. It is measured from the ascending node of Saturn’s equatorial plane on the Earth’s equator at the standard epoch.

Object	Decimal day (UTC) of 1995 November	Distance (km) on equatorial axis	Longitude (degrees)	Filter
A	20.283900	125847	103.7	K
A	20.289005	127699	105.5	K
A	20.293935	131403	109.5	K
A	20.295486	132560	110.9	K
A	20.300613	134875	114.1	K
A	20.301250	135570	115.2	K
A	20.351597	135583	144.3	K
B	20.241563	111493	92.5	H
B	20.243727	113345	93.8	H
B	20.263044	126541	104.3	J
B	20.266250	127930	105.7	J
B	20.266944	128856	106.7	J
B	20.270891	130940	108.9	J
B	20.277755	134412	113.4	J
B	20.337269	133949	146.8	K
B	20.338669	133023	148.0	K
B	20.343287	132097	149.2	K
C	20.214919	136959	117.7	K
C	20.269444	132560	148.6	J
C	20.270359	131403	150.0	J
C	20.272118	130245	151.3	J
C	20.273333	129319	152.3	J
C	20.277755	126541	155.1	J
C	20.288356	120753	160.2	K
C	20.296134	114503	164.9	K
C	20.315706	97139	175.8	K
D	20.248773	128625	153.1	J
D	20.265012	117744	162.5	J
D	20.266250	117281	162.9	J
D	20.267894	115429	164.2	J
D	20.270891	114503	164.9	J
D	20.278275	109409	168.4	J

time baseline, as it is the most important factor for an accurate orbit determination. The CFHT data points are presented in Table 1, in which the filter as well as the current longitude of each object are also reported.

Semi-major axis and longitude at epoch are determined by a least square fit of the position of objects projected onto the equatorial axis of Saturn. Error bars are obtained by introducing a random noise in the input positions, with dispersion equals to the spatial uncertainty ($0.09''$ for CFHT and $0.035''$ for HST).

A circular fit was performed first. The results are presented in Table 2. They confirm that arcs A to D are located between Pandora and Prometheus ($\sim 140\,050$ km). Since such elongated structures are expected to be em-

bedded in the F ring, we also performed a non-circular fit assuming the eccentricity and longitude of pericenter of the F ring, but the residuals did not significantly decrease.

If it is assumed that objects A, B, C, D are embedded in the F ring, an estimate of its semi-major axis in 1995 is calculated by taking the mean semi-major axis. Based on the circular fit we obtain $\langle a \rangle = 140\,060 \pm 60$ km ($\Leftrightarrow n = 582.9 \pm 0.4$ $^\circ/day$), with a physical width of ± 20 km around the mean, calculated by taking the standard deviation of the four derived semi-major axes. For non-circular fit we obtain $\langle a_{ex} \rangle = 140\,050 \pm 60$ km ($\Leftrightarrow n = 583.0 \pm 0.4$ $^\circ/day$), with a physical width of ± 30 km around the mean. Combining both data set allows to significantly im-

Table 2. Orbital fit for A,B,C,D derived by combining HST and CFHT data. The orbital fit for Pandora is also reported as it is detected in both HST and CFHT data (below 80°). The standard epoch is 1995 November 21.5 TDT at Saturn. Longitude is measured from the ascending node of Saturn’s equatorial plane on the Earth’s equator at the standard epoch.

0: Circular orbit.

1: Eccentricity and longitude of pericenter of the F ring at the standard epoch are assumed to be $e=0.0029$ and $\omega=292.5^\circ$ (Synnott et al. 1983).

2: Eccentricity and longitude of pericenter of Pandora are assumed to be $e=0.0044$ and $\omega=274.7^\circ$.

Object	Semi-major axis (km)	Longitude at epoch (degrees)	Residuals (km)	Mean Motion (deg/day)
A ⁰	140 070±166	122.85°±1.3	751	582.92±0.96
B ⁰	140 083±108	135.81°±0.6	617	582.80±0.60
C ⁰	140 050±119	177.32°±0.8	643	583.05±0.68
D ⁰	140 046±141	192.47°±0.9	691	583.07±0.91
A ¹	140 075±158	122.66°±1.2	723	582.89±1.02
B ¹	140 081±100	135.43°±0.6	598	582.85±0.61
C ¹	140 017±109	177.66°±0.5	611	583.23±0.68
D ¹	140 021±139	192.69°±1.0	657	583.23±0.87
Pandora ²	141 792±87	52.0°±0.3	512	572.30±0.53

prove the orbital solution of arc B ($584 \pm 4^\circ/\text{day}$) as reported in N96. This gives also the first determination of the orbits of A,C and D arcs.

4. Discussion

4.1. Comparison with August and November 1995 observations

Another 10° -long arc has been seen by N96 (it is designed here as the “E arc”, see Fig. 2.c) on November 21st 1995. Its orbit has been determined by P2000 using November 17th, 18th and 21st HST images. Their value of $140\,074 \pm 30$ km is consistent (1σ) with the A,B,C and D arcs location.

Some other objects discovered in August 1995, during the Earth crossing seemed also to be close to and somewhat below 140 000 km (Roddier et al. 1996a; N96; Ferrari et al. 1997; P2000). However most of them appeared to be point-like, and thus possibly of a different nature than features A to E. Based on N96 orbital solutions, S6 and S7 are located at 139 900 km and 139 100 km (with error bars of 70 km and 260 km respectively). The orbit of S5 is still a matter of debate (P.D. Nicholson, private communication). Its semi-major was initially estimated as $139\,860 \pm 130$ km by N96 and $140\,050 \pm 100$ km by Roddier et al.(1996a), but two recent studies, combining different data sets, gives incompatible results : P2000 find $140\,208 \pm 50$ km and McGhee et al. (submitted to Icarus) report $a=139\,690 \pm 90$ km. A few other objects (S11 to S19) where also discovered by Roddier et al.(1996a, 1996b). Their estimated orbits are not accurate enough to give us more information on the F ring environment (error bars are ± 1000 km and ± 2000 km for S8 and S9,

and ± 500 km for objects S11 to S15).

4.2. Comparison with 1980-81 Voyager observations

Values of $\langle a \rangle$ and $\langle a_{ex} \rangle$ are however quite far (3σ) from all estimates of the F ring radius derived from Voyager images, by about -150 km. Indeed Synnott et al. (1983) gives $a = 140\,185 \pm 30$ km. A recent study of Voyager images (Ferrari et al. 1997, 1998) reveals that, at the Voyager epoch, some of the brightest structures of the F ring move on different orbits, with a measured dispersion of 95 ± 15 km (1σ). The measured semi-major axis is $140\,219 \pm 19$ km derived from Voyager 1 data and $140\,205 \pm 10$ km derived from Voyager 2 data. All those results are consistent with French and Nicholson who used a different approach based on Voyager and stellar occultation data (unpublished work of French & Nicholson, reported in N96) giving $a=140\,209 \pm 4$ km.

4.3. F ring radial structure

The width of the F ring in Voyager images is up to 300 km and the ring is formed of four eccentric strands (Murray et al.1997), $F\alpha$, $F\beta$, $F\gamma$ and $F\delta$, which radial width is 50 km in average and with respective semi-major axes 140 089 km, 140 176 km, 140 219 km and 140 366 km. The $F\gamma$ strand is by far the brightest and may be the “core” of the F ring with centimeter-sized bodies (Showalter et al. 1992; Murray et al. 1997), in which the brightest features (like clumps or arcs) were detected at the Voyager epoch (Ferrari et al. 1997; Showalter 1997). The five arcs seen in November 1995 (A,B,C,D and E)

seem to be gathered around 140 060 km, close to the the faint $F\alpha$ strand. Consequently, if the 1995 November arcs belong to a F ring core, this may imply a radial restructuring or a spreading of the ring in the meantime.

4.4. Possible implications

We suggest below, as a direction for future works, that some close encounter with one of the shepherding satellites may have reshaped the F ring in the last twenty years. Such an hypothesis may not be excluded since the dynamical evolution of this ring is still a puzzle for the scientific community. The evolution of the F ring may critically depend on its two shepherding satellites, Pandora and Prometheus (see for example: Dermott 1981; Showalter & Burns 1982; Lissauer & Peale 1986). During the 1995 crossings, Prometheus was lagging its expected position by $\sim 19^\circ$ (N96). It has been suggested that an encounter of the F ring with Prometheus may have happened in between 1991 and 1994 (Murray & Giuliatti Winter 1996) due to the precessional variation of the orbits owing to Saturn's oblateness. The dynamical consequence of this encounter on the structure of the F ring is not currently known. It might result in breaking of the strands and in the creation of structures in the inner regions of the F ring. Indeed a massive body is able to scatter its environment inside three Hill's radii (Nishida 1983; Ida & Makino 1993) that is about 300 km for Prometheus (assuming a mass ratio of $\sim 10^{-9}$ between Prometheus and Saturn). Then in case of an instantaneous close approach to the F ring, estimated at ~ 50 km (Murray & Giuliatti Winter 1996), Prometheus might be able to perturb the ring over a distance of 300 km, i.e. about the full width of the F ring. Such a model has been recently considered (abstract of Showalter et al. 1999; P.D. Nicholson, private communication), and first results show that Prometheus may perturb a portion of the F ring after each close encounter. However the resulting radial displacement seems to be about 1 kilometer only.

In addition, during the interaction, Prometheus at its apocenter is close to the F ring's pericenter, yielding strong relative velocities of ~ 30 m/s. Such high-velocity encounters may result in catastrophic disruption of bodies initially in the F ring. The inner region of the F ring may be consequently populated with fragments especially if a belt of kilometer-sized moonlets exists between Prometheus and Pandora, as originally suggested by Cuzzi & Burns (1988).

5. Conclusion

We have reported observations of the crossing of Saturn's ring-plane by the Sun, on 1995 November 20th, made with the 3.6m CFH Telescope, using the UHAO adaptive optics system. Four azimuthally extended structures (A,B,C,D)

have been detected, with central longitude at epoch of 123° , 136° , 177° and 193° (see Table 2), on 1995 November 21.5 TDT at Saturn. These structures have been also seen one day later in HST images (N96). The combination of both CFHT and HST data sets provides an accurate estimate of their orbit. A circular orbital fit locates them between 140 020 km and 140 080 km, with error bars of 120 km on average. The mean circular orbit is $140\,060 \pm 60$ km, that is consistent with the orbit of another bright arc observed at the same epoch (P2000). However, this represents a significant discrepancy (3σ) with previous estimates of the F ring's radius derived from Voyager images (located at 140 200 km on average). If the five arcs observed in November 1995 belong to a F ring core, this would imply a radial restructuring or a spreading of the F ring between 1980 and 1995, whose explanation has still to be found. In order to understand the F ring's dynamics, better spatial resolution and longer time baselines observations are required. The Cassini encounter in 2004 will probably be a major step in the understanding of the F ring mysteries.

Acknowledgements. The authors thank P.D. Nicholson for his helpful comments, as a referee.

References

- Bosh, A.S., Rivkin, A.S., 1996, *Science* 272, 518
- Cuzzi, J.N., Burns J.A., 1988, *Icarus* 74, 284
- Campbell, J.K., Anderson, J.D., 1989, *AJ* 97, 1485
- Dermott, S.F., 1981, *Nature* 290, 454
- Ferrari, C., Brahic, A., Charnoz, S., Thébault, P., Roddier F., 1997, *BAAS* 29, 998
- Ferrari, C., Brahic, A., Charnoz, S., Thébault, P., 1998, *Actes du deuxième colloque national de planétologie de l'INSU*, Vol. 2, 57.5
- Holtzman, J.A., Burrows, C.J., Casertano, S., Hester, J.J., Trauger, J.T., Watson, A.M., Worthey, G., 1995. *Pub. Astron. Soc. Pacific* 107, 156
- Ida, S., Makino, J., 1993, *Icarus* 106, 210
- Lissauer, J.J., Peale S.J., 1986, *Icarus* 67, 358
- Murray, C.D., Giuliatti Winter, S.M., 1996, *Nature* 380, 139
- Murray, C.D., Gordon, M.K., Giuliatti Winter, S.M., 1997, *Icarus* 129, 304
- Nicholson, P.D., Showalter, M.R., Dones, L., French, R.G., French, R.G., Larson, M., Lissauer, J., McGhee, C.A., Seitzer, P., Sicardy, B., Danielson, E.G., 1996, *Science* 272, 509
- Nishida, S., 1983, *Prog. Theor. Phys.* 70, 93
- Poulet, F., Sicardy, B., Nicholson, P. D., Karkoschka, E. and Caldwell, J. 2000, *Icarus*, 144, 135
- Porco, C., Danielson, G. E., Goldreich, P., Holberg, J. B. and Lane, A. L. 1984, *Icarus*, 60, 17
- Roddier, C., Roddier, F., Brahic, A., Graves, J.E., Northcott, M.J., Owen, T., Thébault, P., 1996.a, *IAU circ* 6407
- Roddier, C., Roddier, F., Brahic, A., Graves, J.E., Northcott, M.J., Owen, T., Thébault, P., 1996.b, *IAU circ* 6515
- Roddier, F., Roddier, C., Brahic, A., Dumas, C., Graves, J. E., Northcott, M. J. and Owen, T. 2000, *Icarus*, 143, 299

- Showalter, M. R. and Burns, J. A. 1982, *Icarus*, 52, 526
- Showalter, M. R., Pollack, J. B., Ockert, M. E., Doyle, L. R.
and Dalton, J. B. 1992, *Icarus*, 100, 394
- Showalter, M.R. 1997, *BAAS* 29, 999
- Showalter, M.R., Dones, L., Lissauer, J.J. 1999, *BAAS* 31, 1141
- Sicardy, B., Poulet, F., Beuzit, J-L., and Prado, P., 1996,
IAU circ 6395
- Synnott, S.P., Terrile, R.J., Jacobson, R.A., Smith, B.A., 1983,
Icarus 53,156